Journal of Controlled Release 393 (2026) 114830

Contents lists available at ScienceDirect

Journal of Controlled Release

journal homepage: www.elsevier.com/locate/jconrel

Tunable microgel modulars for temporally coordinated combination therapy

Zhisheng Xiao [a,b], Zhiqiang Wu [c], Qiaofeng Li [b], Yu Miao [b], Nan Wang [a], Yifang Yang [b], Qian Chen [b,*], Yang Yang [a,c,**]

[a] Department of Thoracic Surgery, The Fourth Affiliated Hospital of Soochow University, Suzhou, Jiangsu 215123, China
[b] Institute of Functional Nano & Soft Materials (FUNSOM), Jiangsu Key Laboratory for Carbon-Based Functional Materials and Devices, Soochow University, Suzhou 215123, China
[c] Department of Thoracic Surgery, Shanghai Pulmonary Hospital, School of Medicine, Tongji University, Shanghai 200433, China

ARTICLE INFO

Keywords:
Microgel
LEGO-inspired
Modular drug delivery
Programmable release
Sequential therapy

ABSTRACT

Hydrogels are widely used in local drug delivery, however, achieving independent and programmable release of multiple drugs from a single formulation remains a major challenge, particularly for combination therapies requiring precise temporal coordination. Inspired by the customizable assembly of LEGO bricks, we developed an injectable modular microgel platform for programmable multi-drug delivery by combining distinct microsphere modules—each optimized for specific drug types. For example, Gelatin methacrylate microspheres for hydrophilic drugs and Alginate microspheres for hydrophobic drugs. The resulting composite microgel exhibits outstanding injectability, rapid self-healing properties, and prolonged in vivo retention, ensuring stable and sustained drug delivery. By modulating matrix concentrations, we achieved precise tuning of release profiles across a broad spectrum of therapeutic agents, from small molecules to large proteins. We demonstrated clinical potential in two applications: (1) Sequential delivery of carboplatin followed by RSL3 overcame chemotherapy resistance, extending mouse survival by 10 days compared to conventional hydrogels. (2) Controlled release of doxorubicin and paclitaxel leveraged their distinct mechanisms to eliminate cancer cells, reducing tumor mass 3.53-fold versus traditional hydrogels. This modular microgel strategy transcends the limitations of conventional monolithic systems by enabling the independent programming of drug release profiles, offering a versatile and customizable platform for implementing sophisticated temporal combination therapies with enhanced precision and therapeutic outcomes.

1. Introduction

Hydrogels have emerged as a premier platform for localized and sustained drug delivery due to their biocompatibility, high hydration capacity, and tunable physical properties [1,2]. These three-dimensional polymer networks function as reservoirs, enabling controlled release of encapsulated therapeutics via diffusion and matrix degradation, thereby maintaining optimal drug concentrations at targeted sites and improving therapeutic efficacy [3–6]. However, most hydrogel-based delivery systems remain fundamentally monolithic, relying on a single matrix to control all encapsulated agents simultaneously. This architectural simplicity imposes a critical limitation: the inability to independently regulate the release kinetics of multiple drugs from a single formulation [7,8]. Typically, such systems exhibit simplistic release kinetics—characterized by an initial burst followed by a gradual decline—rendering them unsuitable for complex, multi-drug regimens [9]. This limitation is particularly critical in modern combination therapies that require precise timing, sequence, or duration of drug exposure [10,11]. Moreover, co-encapsulation of drugs with divergent properties, such as hydrophilic and hydrophobic compounds, in a single matrix often results in incompatible loading efficiencies and compromised release profiles [12,13]. Consequently, traditional hydrogels lack the precision required for sequential drug delivery, where the timing and order of drug release are crucial for achieving synergistic therapeutic effects [14–19].

Drawing inspiration from the modular design principle of LEGO

* Corresponding author.
** Corresponding author at: Department of Thoracic Surgery, The Fourth Affiliated Hospital of Soochow University, Suzhou, Jiangsu 215123, China.
E-mail addresses: chenqian@suda.edu.cn (Q. Chen), timyangsh@tongji.edu.cn (Y. Yang).

https://doi.org/10.1016/j.jconrel.2026.114830
Received 9 December 2025; Received in revised form 16 January 2026; Accepted 14 March 2026
Available online 15 March 2026

bricks, where standardized units can be flexibly assembled into complex architectures, we developed an innovative modular microgel platform to address current challenges in drug delivery. This system features independently engineered microsphere modules with precisely controlled. Firstly, Gelatin methacrylate (GelMA) microspheres were fabricated via microfluidics for hydrophilic drugs delivery module and Alginate (ALG) microspheres were produced through electrospray for hydrophobic drug delivery module. Our results demonstrate that the release profile of each drug can be precisely tuned by adjusting the matrix concentration of its corresponding module, as validated using model compounds ranging from small molecules to proteins. Moreover, these modular components can be seamlessly integrated into an injectable composite microgel system that exhibits exceptional shear-thinning and self-healing properties, allowing for smooth syringe injection and perfect conformal filling of target tissues.

To demonstrate the clinical potential of this modular platform, we provided two distinct therapeutic implementations that showcase its versatility and superior performance. Firstly, we engineered a sequential

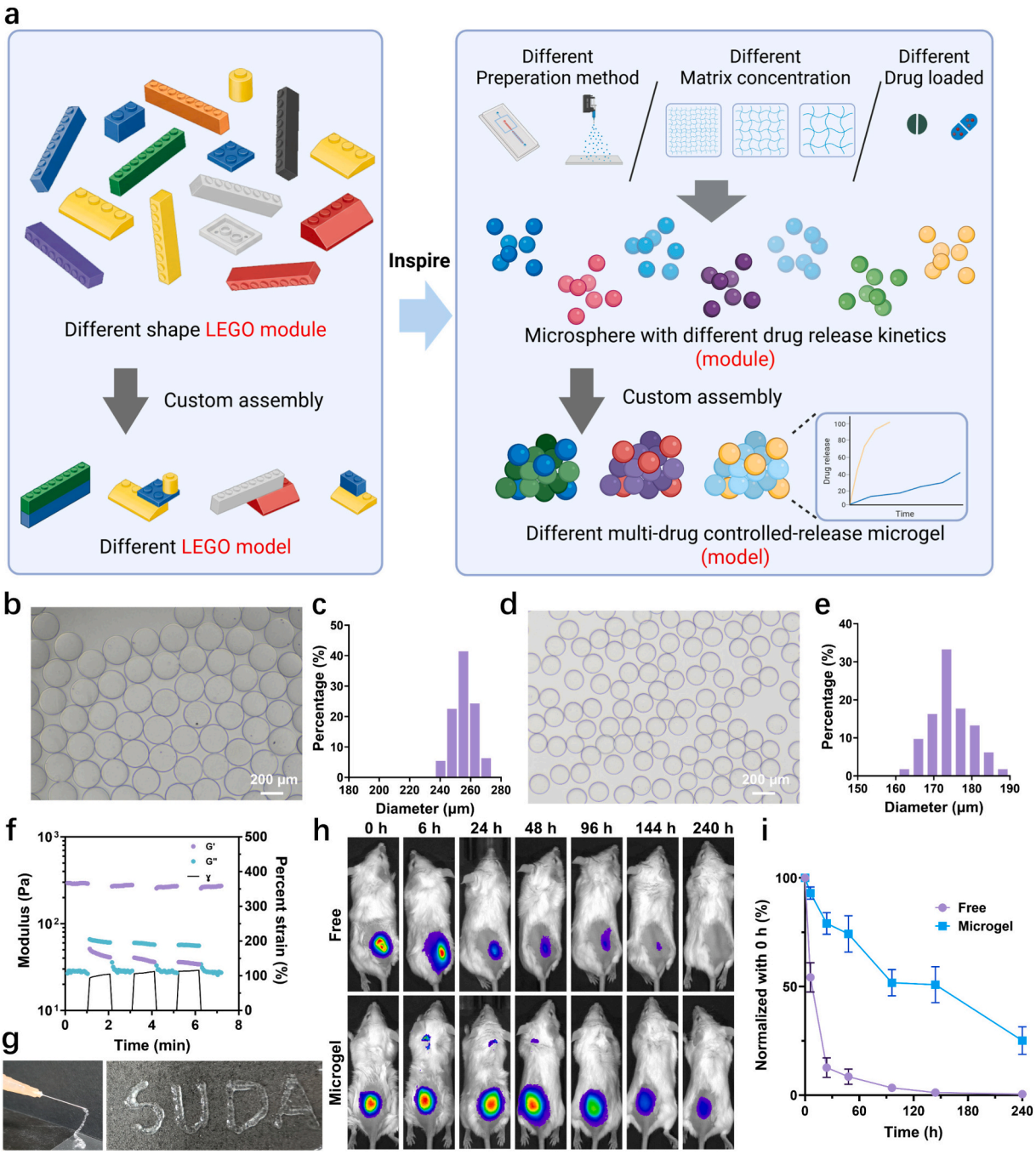

Fig. 1. Preparation and characterization of LEGO microgel (a) Schematic illustration of the LEGO-inspired modular microsphere system, where microspheres with tunable drug release profiles are fabricated through different methods and concentrations, independently loaded with distinct drugs, and flexibly assembled like LEGO® bricks to create programmable microgel constructs for controlled multi-drug delivery. (b, c) The bright-field imaging (b) and the statistics of the diameter (c) of GelMA microsphere prepared by microfluidics. (d, e) The bright-field imaging (d) and the statistics of the diameter (e) of ALG microspheres prepared by the electrospray. (f) Strain-cycle experiment for combined GelMA/ALG microgel, whereby materials are cycled between 0.5% and 100% (shaded) strains. (g) Injection of the combined GelMA/ALG microgel from a syringe through a 24 G needle. (h, i) In vivo fluorescence imaging (h) and the corresponding semiquantitative analysis (i) of mice subcutaneous injection of cyanine5.5 (Cy5.5) labelled microgel or free Cy5.5 at different time points ($n = 3$). The data are presented as mean ± sem.

drug delivery system to address platinum-based chemotherapy resistance [20]. The optimized microgel formulation achieves rapid carboplatin release to initiate tumor cell apoptosis, followed by sustained RSL3 delivery that effectively targets drug-tolerant persister cells, achieving significantly improved therapeutic efficiency, extend the survival period of mice by up to 10 days over conventional bulk hydrogel. Secondly, we reconfigured the modular components to replicate the clinical DOX/PTX regimen [21,22], successfully implementing a precisely timed-release profile featuring immediate DOX delivery, which effectively killed S-phase cancer cells [23], coupled with extended PTX release, further killed M-phase cells [24], and reduced the systemic toxicity. The optimized formulation demonstrated significantly enhanced antitumor efficacy compared to standard bolus injections, evident by 3.53-fold less tumor weight, validating the platform's ability to recapitulate and improve upon complex clinical treatment protocols. Therefore, this LEGO-inspired modular strategy presents a paradigm shift in drug delivery design—from single-matrix formulations toward programmable, mix-and-match delivery systems capable of orchestrating complex, temporally coordinated combination therapies that are inaccessible to conventional hydrogels.

1.1. Fabrication and characterization of LEGO-inspired modular microgels

Inspired by the modular assembly of LEGO bricks into diverse structures, we developed LEGO-like microspheres with tunable drug release profiles by precisely tailoring their preparation method, matrix composition, and concentration (Fig. 1a). Mimicking LEGO brick integration, these modular microspheres were then assembled into composite microgels capable of controlled multi-drug delivery. We firstly fabricated the microspheres (modular) using two distinct techniques: microfluidics and electrospray. GelMA microspheres prepared via microfluidics displayed highly uniform morphology and a narrow size distribution, with an average diameter of 255 μm (Fig. 1b, c). Similarly, ALG microspheres generated by electrospraying exhibited excellent size consistency, averaging 173 μm with minimal variation (Fig. 1d, e).

By integrating these modular microspheres, we engineered an injectable microgel with tunable rheological properties. To evaluate its injectability, we performed oscillatory rheometry under alternating high (100%) and low (0.5%) strain conditions (Fig. 1f). At low strain, the combined GelMA/ALG microgel exhibited solid-like behavior, with a storage modulus ($G' \approx 300$ Pa) exceeding the loss modulus ($G'' \approx 27$ Pa) by an order of magnitude. When subjected to high strain, it exhibited rapid shear-thinning behavior, as G' decreased to 50 Pa, falling below G'' (≈60 Pa), indicating reversible fluidization. Moreover, the combined GelMA/ALG microgel flowed smoothly through 23-gauge needles and retained sufficient post extrusion to maintain customized shapes (Fig. 1g), confirming its dual functionality as both an injectable and moldable drug delivery platform.

To evaluate the microgel's potential as a sustained-release drug carrier, we performed in vivo retention studies by loading it with Nile Red and administering it subcutaneously in mice, with free dye serving as a control. Fluorescence imaging and semi-quantitative analysis (Fig. 1h, i) demonstrated striking differences in retention kinetics: while the free dye signal rapidly diminished within 48 h and became nearly undetectable thereafter, the microgel-encapsulated dye exhibited progressive signal decay, maintaining detectable fluorescence up to 10 days post-administration. These results clearly demonstrate the microgel's superior retention capability and its potential for sustained release.

1.2. Independent drug release kinetics from modular microspheres

To characterize the drug release behavior of individual microsphere components within the microgel system, we employed distinct encapsulation strategies based on drug solubility. For hydrophilic drugs, we utilized microfluidic fabrication of GelMA microspheres, where drugs were dissolved in the internal aqueous phase, which achieved high loading efficiency by leveraging the drug's insolubility with the external oil phase (Fig. 2a). Conversely, for hydrophobic drugs, we used electrospraying technique to produce ALG microspheres, incorporating the drugs directly into the ALG precursor prior to crosslinking in calcium chloride solution, thereby minimizing aqueous-phase drug leakage (Fig. 2b).

To systematically evaluate hydrophilic drug release kinetics, we employed three model compounds with increasing molecular weights. Using Rhodamine (MW: 0.48 kDa) as a small molecule model, we observed rapid initial release from 2.5% GelMA (complete release within 12 h), while 5% and 7.5% GelMA progressively slowed the release profile (Fig. 2c). After 12 h, both 2.5% and 5% groups approached complete release, whereas the 7.5% group exhibited sustained retention (~80% cumulative release, Fig. 2d), demonstrating concentration-dependent but molecular weight-limited diffusion control. To assess larger hydrophilic compounds, we employed 4 kDa dextran, which exhibited significantly improved retention across all GelMA (Fig. 2e). The 12-h cumulative release decreased systematically with increasing GelMA concentration (77.2% at 2.5%, 67.5% at 5%, and 57.1% at 7.5%, Fig. 2f), highlighting enhanced matrix entrapment for higher MW molecules. For protein delivery, BSA (MW: 66.4 kDa) encapsulation revealed even more pronounced sustained release behaviors (Fig. 2g). Due to substantial size exclusion effects, the 12-h cumulative release was further reduced to 52.6%, 45.4%, and 41.6% from 2.5%, 5%, and 7.5% GelMA microspheres, respectively (Fig. 2h).

To characterize hydrophobic drug release kinetics, we encapsulated Nile Red within electrosprayed ALG microspheres. The release profiles demonstrated sustained, concentration-dependent release under physiological conditions (Fig. 2i). Over 20 days, cumulative release systematically decreased with increasing ALG concentration, reaching only 51.6% (0.5% ALG), 18.4% (1%), and 9.4% (1.5%) (Fig. 2j). This concentration-dependent release pattern was further validated using the moderately hydrophobic dye Cy5.5 (Fig. 2k). By day 10, cumulative release values exhibited a similar inverse correlation with matrix density (85.4% at 0.5%, 64.3% at 1%, and 43.9% at 1.5% ALG) (Fig. 2l). These results collectively demonstrate precise tunability of hydrophobic drug release through simple modulation of ALG matrix concentration.

1.3. Superior efficacy of modular drug delivery

To highlight the programmatic delivery advantages of our modular carrier system, we employed a “chemotherapy-induced drug resistance reversal” sequential treatment paradigm as our proof-of-concept model. This therapeutic strategy capitalizes on the mechanistic interplay where platinum-based chemotherapeutics (such as carboplatin, CBP) exert cytotoxic effects while simultaneously upregulating GPX4 expression, thereby fostering the emergence of drug-tolerant “persistent tumor cells” [25–27]. These resilient populations can then be effectively eradicated by the GPX4 inhibitor RSL3 [28] (Fig. 3a). Our systemic validation began with in vitro confirmation of drug synergy. Western blot analysis (Fig. 3b) demonstrated that while CBP treatment moderately elevated GPX4 protein levels, RSL3 administration potently suppressed its enzymatic activity. Flow cytometry evaluation of the persister cell markers CD133 [29,30] and ALDH [31] activity revealed a striking increase in $CD133^{+}$ populations and ALDH activity post-CBP exposure, which was dramatically revealed upon RSL3 co-treatment (Fig. 3c, Supporting information 1), confirming RSL3's efficacy in eliminating chemotherapy-induced resistant clones. Dose-response profiling through MTT assays yielded critical insights: whereas only supraphysiological CBP concentrations (160 μM) exhibited significant cytotoxicity and RSL3 monotherapy showed negligible toxicity, pretreatment with physiologically relevant CBP doses (10 μM) rendered cells exquisitely sensitive to RSL3 (Fig. 3d, e). Besides, the sensitization effect exhibited a distinct dose-dependent relationship with CBP. At a lower CBP concentration (5 μM), higher RSL3 levels were required to

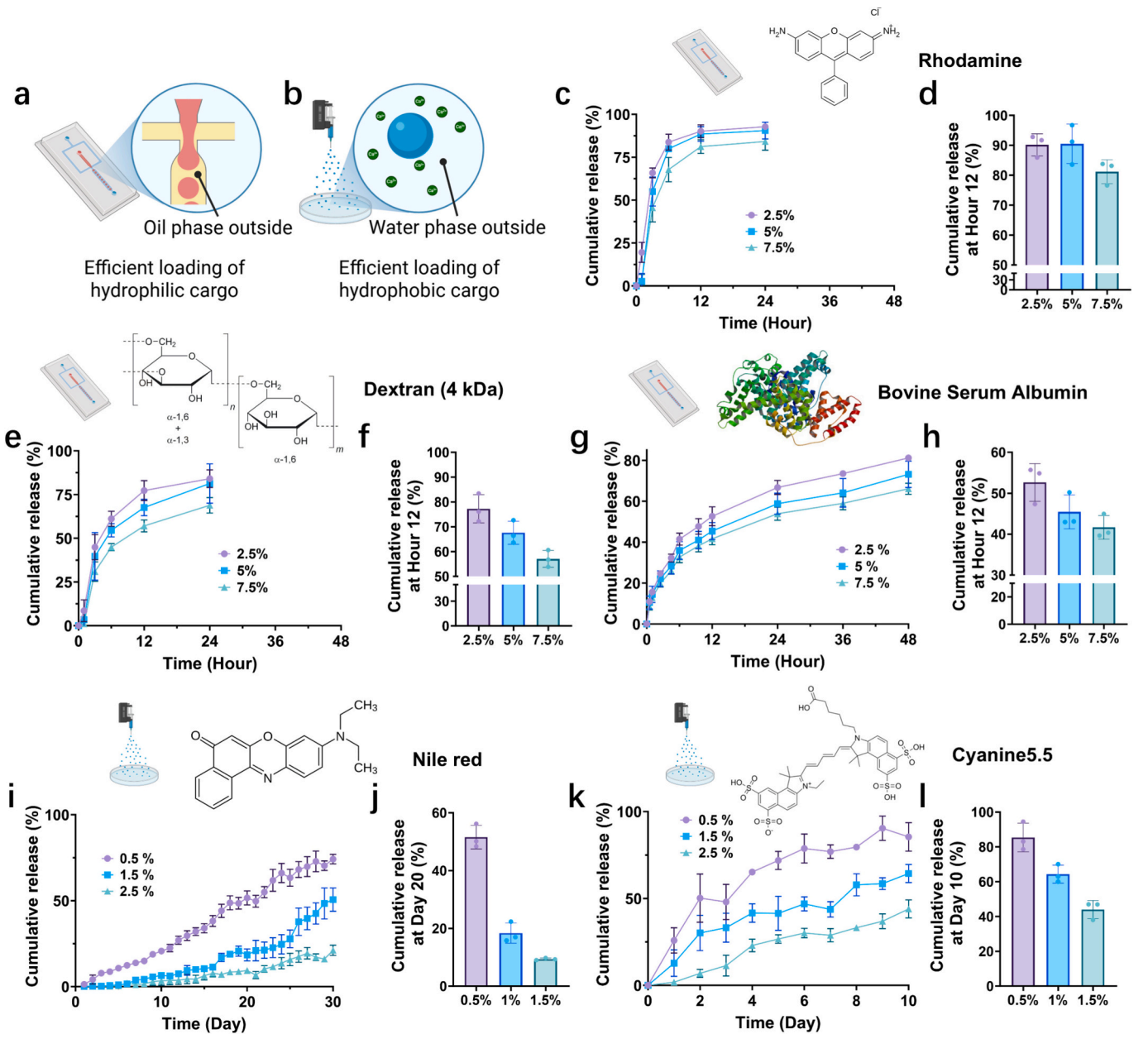

Fig. 2. Controlled drug release from LEGO moduler (a) A schematic illustration showing the microfluidic approach for preparing microspheres loaded with hydrophilic drugs. (b) A schematic illustration showing the electrostatic spraying approach for preparing microspheres loaded with hydrophobic drugs. (c, d) Release curves (c) and 12-h release percentages (d) of rhodamine from GelMA microspheres with varying concentrations (n = 3). (e, f) Release curves (e) and 12-h release percentages (f) of dextran from GelMA microspheres with varying concentrations (n = 3). (g, h) Release curves (g) and 12-h release percentages (h) of bovine serum albumin (BSA) from GelMA microspheres with varying concentrations (n = 3). (i, j) Release curves (i) and 20-day release percentages (j) of nile red from ALG microspheres with varying concentrations (n = 3). (*k*,*l*) Release curves (k) and 20-day release percentages (l) of Cyanine5.5 from ALG microspheres with varying concentrations (n = 3). The data are presented as mean ± sem. (For interpretation of the references to colour in this figure legend, the reader is referred to the web version of this article.)

induce significant cytotoxicity. In contrast, a higher CBP concentration (20 μM) dramatically enhanced RSL3 potency, with even 5 nM RSL3 eliciting substantial cell killing (Supporting information 2). These results delineate a precisely timed therapeutic sequence: initial CBP-mediated tumor debulking and resistant cell generation, followed by RSL3-mediated persister cell ablation, culminating in comprehensive tumor eradication. This temporal synergy underscores the imperative for a delivery platform capable of orchestrating precise drug release kinetics.

To operationalize this sophisticated therapeutic choreography, we used the modular microgel system employing LEGO-like assembly principles. The system's ingenuity resides in its capacity for independent optimization of two distinct microsphere formulations tailored respectively for hydrophilic CBP and hydrophobic RSL3 drugs, subsequently unified into a single injectable therapeutic platform. For the CBP module, we employed microfluidic-generated GelMA microspheres, which demonstrated superior drug loading efficiency compared to ALG hydrogels (Fig. 3f). By systematically adjusting the matrix concentration, we found that increasing GelMA concentration from 2.5% to 7.5% progressively slowed CBP release through hydrogel network densification, thereby extending drug delivery (Fig. 3g). The 7.5% GelMA formulation was ultimately selected as it provided an optimal balance between initial drug concentration and sustained release, preventing early depletion. For the RSL3 module, we utilized electrosprayed ALG

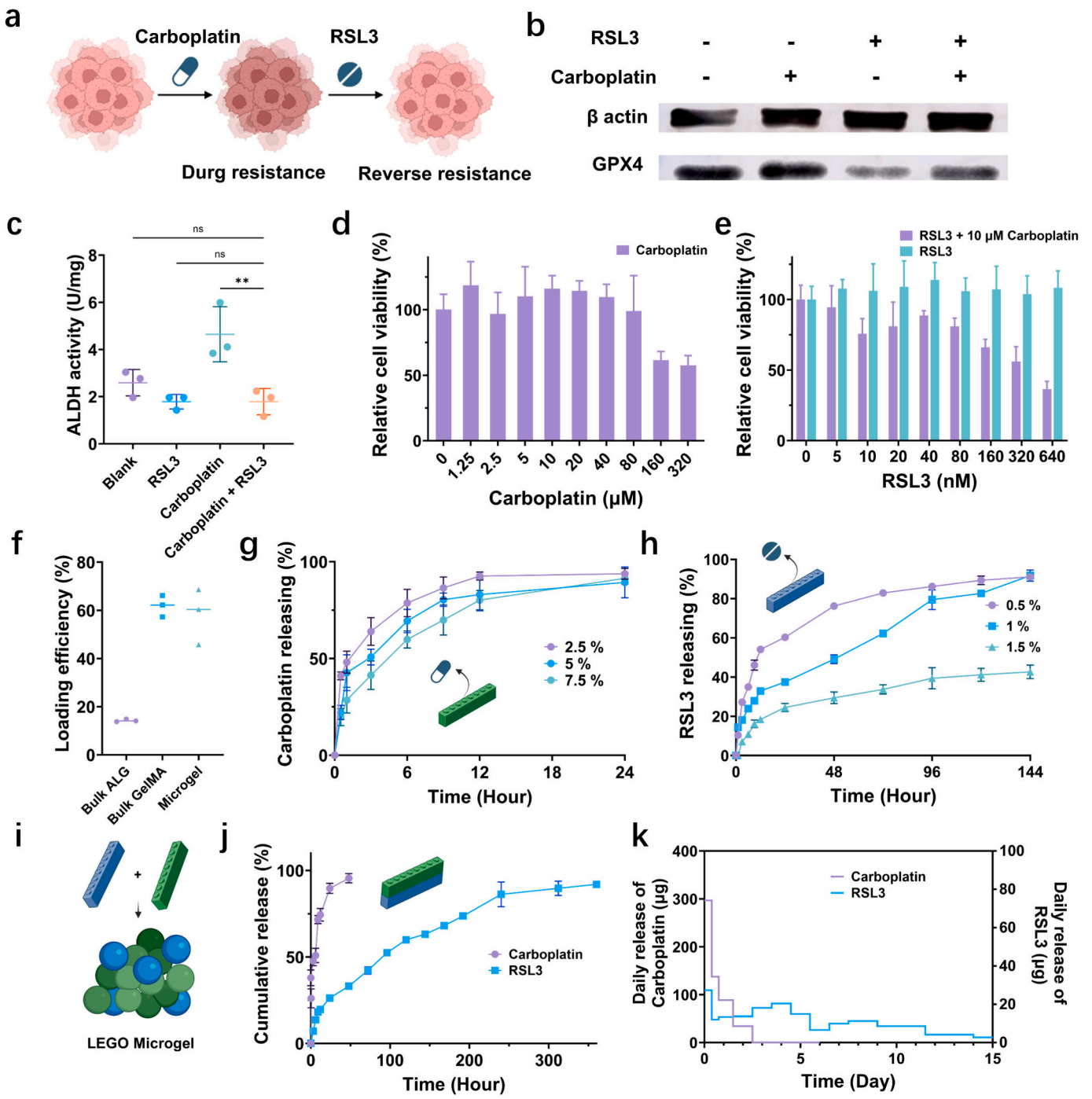

Fig. 3. Mechanism and in vitro validation of CBP/RSL3 combination therapy (a) A schematic of carboplatin-induced GXP4 upregulation (mediating drug resistance) and RSL3-mediated sensitization. (b) Western blot analysis of GPX4 expression in 4 T1 cells under different treatments. (c) Relative viabilities of 4 T1 cells after incubation with carboplatin at different concentrations for 24 h (n = 3). (d) Relative cell viabilities of 4 T1 cells after incubation with RSL3 at different concentrations with or without 10 μM carboplatin for 24 h ($n = 5$). (e) Acetaldehyde dehydrogenase activity in supernatants of 4 T1 cells with different treatments (n = 5). (f) The loading efficiency of carboplatin in different prepared methods of hydrogel (n = 3). (g) The release curves of carboplatin from GelMA microgel with different concentrations (n = 3). (h) The release curves of RSL3 from ALG microgel with different concentrations (n = 3). (i) Schematic illustration showing the assembly process of customizable LEGO-like microgels: individual LEGO-like modules composed of microspheres encapsulated with different drugs are mixed and assembled to simulate the custom construction of LEGO bricks. (j) The release curves of carboplatin and RSL3 from LEGO microgel (n = 3). (k) Daily drug release from LEGO microgel. The data are presented as mean ± sem, and P values were calculated by one-way ANOVA with Tukey's post hoc test, $^{**}p < 0.01$.

microspheres. Similar to GelMA higher matrix concentrations resulted in extended RSL3 release durations. We selected 1.5% ALG concentration to achieve a sustained, near-linear release profile — a critical feature for long-term suppression of persister cells (Fig. 3h).

The key innovation is illustrated in Fig. 3i: the precise physical integration of these pre-programmed modules into a "LEGO Microgel" activates the desired sequential drug release kinetics from a single injection. The composite microgel demonstrated a loading capacity of 132.33 ± 7.3 μg carboplatin per mg microgel and 44.9 ± 3.8 μg RSL3 per mg microgel (Supporting information 3). The composite microgel first delivers rapid CBP release to initiate tumor killing and persister cell induction, followed by sustained RSL3 release to eradicate the resistant

population (Fig. 3j, k). This modular design demonstrated clear functional superiority over conventional delivery systems. To validate efficacy, we employed a Transwell co-culture model with 4 T1 cells (Fig. 4a). Comparative analysis of the dual-drug LEGO microgel (CBP + RSL3) against single-drug controls (CBP-only or RSL3-only) and a conventional bulk hydrogel co-loaded with both drugs revealed striking differences. Cytotoxicity assays (Fig. 4b) showed that while single-drug microgels showed minimal cytotoxicity, the LEGO microgel (CBP + RSL3) induced significant cell death, highlighting the critical role of sequential drug release enabled by our modular system. In contrast, the conventional bulk hydrogel exhibited limited efficacy, likely due to its inability to efficiently release hydrophobic drugs RSL3, thereby compromising drug synergy.

Flow cytometric analysis of $CD133^{+}$ persister cells provided further mechanistic insights (Fig. 4c, d). As anticipated, CBP-only treatment significantly expanded this resistant population. While the Bulk(CBP + RSL3) showed partial reduction, it failed to normalize persister cell levels. Remarkably, the LEGO Microgel(CBP + RSL3) completely prevented persister cell induction, maintaining baseline level comparable to untreated controls. This demonstrates that our modular system effectively delivers functional RSL3 to eliminate therapy- resistant cells. To investigate the underlying ferroptosis mechanism, we monitored lipid peroxidation using the specific fluorescent probe (LiperFluo) [32] (Fig. 4e-g). Both RSL3-only and LEGO Microgel groups exhibited strong fluorescence signals, confirming successful GPX4 inhibition and consequent lipid peroxide accumulation. In contrast, the bulk hydrogel showed markedly weaker signal intensity, visually demonstrating its impaired RSL3 release capability. These findings correlate perfectly with our cytotoxicity and persister cell data, establishing that our modular design enables mechanistically precise combination therapy rather than simply representing a formulation improvement.

1.4. Validated therapeutic efficacy in vivo

We further evaluated the antitumor efficacy of the LEGO Microgel (CBP + RSL3) in the 4 T1 tumor-bearing mouse model. All microgel formulations including Microgel(CBP) (containing 30 mg/kg carboplatin), Microgel(RSL3) (containing 10 mg/kg RSL3)and LEGO Microgel (CBP + RSL3) (containing 30 mg/kg carboplatin and 10 mg/kg RSL3) were administered via intratumoral injection, while the bulk hydrogel loaded with CBP and RSL3 (Bulk(CBP + RSL3)) group (containing 30 mg/kg carboplatin and 10 mg/kg RSL3) received peritumoral subcutaneous implantation due to its non-injectable nature (Fig. 4h). However, the elevated interstitial pressure in solid tumors drives the outward diffusion of intratumorally injected material, resulting in significant overlap between the two formulations' effective drug delivery volumes in the critical peritumoral region. Tumor growth curves and survival analyses revealed distinct therapeutic outcomes across different groups (Fig. 4i, j, Supporting information 4). The Microgel(CBP) group exhibited initial tumor suppression, but its efficacy was transient, likely due to late-stage recurrence driven by carboplatin-induced drug-resistant cell populations. In contrast, the Microgel(RSL3) group exhibited tumor progression similar to the blank control, consistent with RSL3's limited intrinsic cytotoxicity against tumor cells. The Bulk(CBP + RSL3) group displayed only modest improvement over carboplatin monotherapy, attributable to its sluggish RSL3 release kinetics. Remarkably, the LEGO Microgel(CBP + RSL3) group achieved the most pronounced tumor growth inhibition and significantly prolonged survival. This superior performance stems from the modular design, which enables precise tuning of RSL3 release rates to synergize with carboplatin's therapeutic activity.

To investigate the mechanistic basis for observed therapeutic differences, we analyzed tumor tissues harvested 15 days post-treatment via Western blot and immunofluorescence staining. GPX4 protein expression was significantly suppressed exclusively in the Microgel (RSL3) and LEGO Microgel(CBP + RSL3) groups, while levels in the Bulk (CBP + RSL3) group remained comparable to the control group (Fig. 4k). These findings confirm that only the modular microgel system enables effective RSL3 delivery to the target site for full pharmacological activity. Immunofluorescence staining for the persistent tumor marker CD133 revealed widespread $CD133^{+}$ cell populations in the Microgel (CBP) group, whereas both the LEGO Microgel(CBP + RSL3) and Microgel(RSL3) groups exhibited minimal positivity (Fig. 4l, Supporting information 5). Together, these results demonstrate that our modular LEGO microgel system achieves precise temporal coordination of two critical therapeutic phases: carboplatin-induced tumor sensitization and RSL3-mediated clearance, which overcomes the efficacy limitations of conventional formulations, enabling synergistic antitumor effects in complex in vivo environments.

1.5. Precise delivery of clinical sequential chemotherapy regimens

To further demonstrate the broad therapeutic potential of our modular delivery platform, we extended our investigation to a clinically pivotal chemotherapy sequence: the sequential administration of anthracyclines followed by taxanes in breast cancer treatment [33,34]. This well-established regimen, supported by robust clinical evidence and meta-analyses (EBCTCG), has demonstrated superior survival outcomes and reduced toxicity compared to concurrent administration [35]. The development of a single-administration system capable of precisely replicating this temporal drug release profile—sustained DOX release followed by PTX—would represent a transformative advancement in clinical oncology. Building upon our successful LEGO microgels platform, we engineered independent drug release modules for DOX and PTX through systematic optimization of matrix compositions.

To achieve the desired sequential drug release profile, we developed two distinct functional modules through precision engineering approaches. For DOX module, microfluidic technology was employed to prepare GelMA microspheres at varying polymer concentrations (2.5%–7.5%). Systemic release studies demonstrated that 7.5% GelMA microspheres exhibited optimal sustained release kinetics, extending the DOX release window while maintaining therapeutic concentrations, thereby ensuring adequate initial tumor exposure (Fig. 5a). For the PTX module, we adopted an alternative strategy using electrospray techniques to prepare ALG microspheres (0.5%–1.5%). In contrast to our previous RSL3 encapsulation approach, we selected 0.5% ALG microspheres to facilitate rapid drug liberation (Fig. 5b). The integration of these independently optimized modules through simple physical mixing yielded LEGO Microgels(DOX + PTX), in which the loading capacity was determined to be 47.9 ± 3.1 μg doxorubicin per mg microgel and 22.9 ± 2.6 μg peclitaxel per mg microgel (Supporting information 6), have precisely recapitulated the clinically validated pharmacokinetic profile (Fig. 5c, d). This successful replication of complex clinical pharmacokinetics through rational modular design conclusively demonstrates our platform's capability for programmable spatiotemporal drug delivery.

To evaluate the therapeutic potential of our sequential delivery system, we conducted comprehensive studies in the 4 T1 subcutaneous tumor model, with intratumoral injection of Microgel(DOX) (containing 10 mg/kg DOX), Microgel(PTX) (containing 5 mg/kg PTX) and LEGO Microgel(DOX + PTX) (containing 10 mg/kg DOX and 5 mg/kg PTX), and peritumoral subcutaneous implantation of Bulk(DOX + PTX) (containing 10 mg/kg DOX and 5 mg/kg PTX). The results demonstrated striking therapeutic advantages of the modular approach. Quantitative tumor volume analysis revealed that only the LEGO Microgel (DOX + PTX) group exhibited significant tumor growth inhibition through the 22-day observation period (Fig. 5e, h-l). In contrast, all control groups including single-drug microgels and conventional bulk hydrogels, exhibited comparable tumor growth kinetics, underscoring the critical importance of our sequential release strategy. Notably, the optimized drug release profile of the LEGO Microgel system translated to exceptional safety characteristics. Body weight monitoring showed no significant fluctuations in the treatment group (Fig. 5g), confirming the

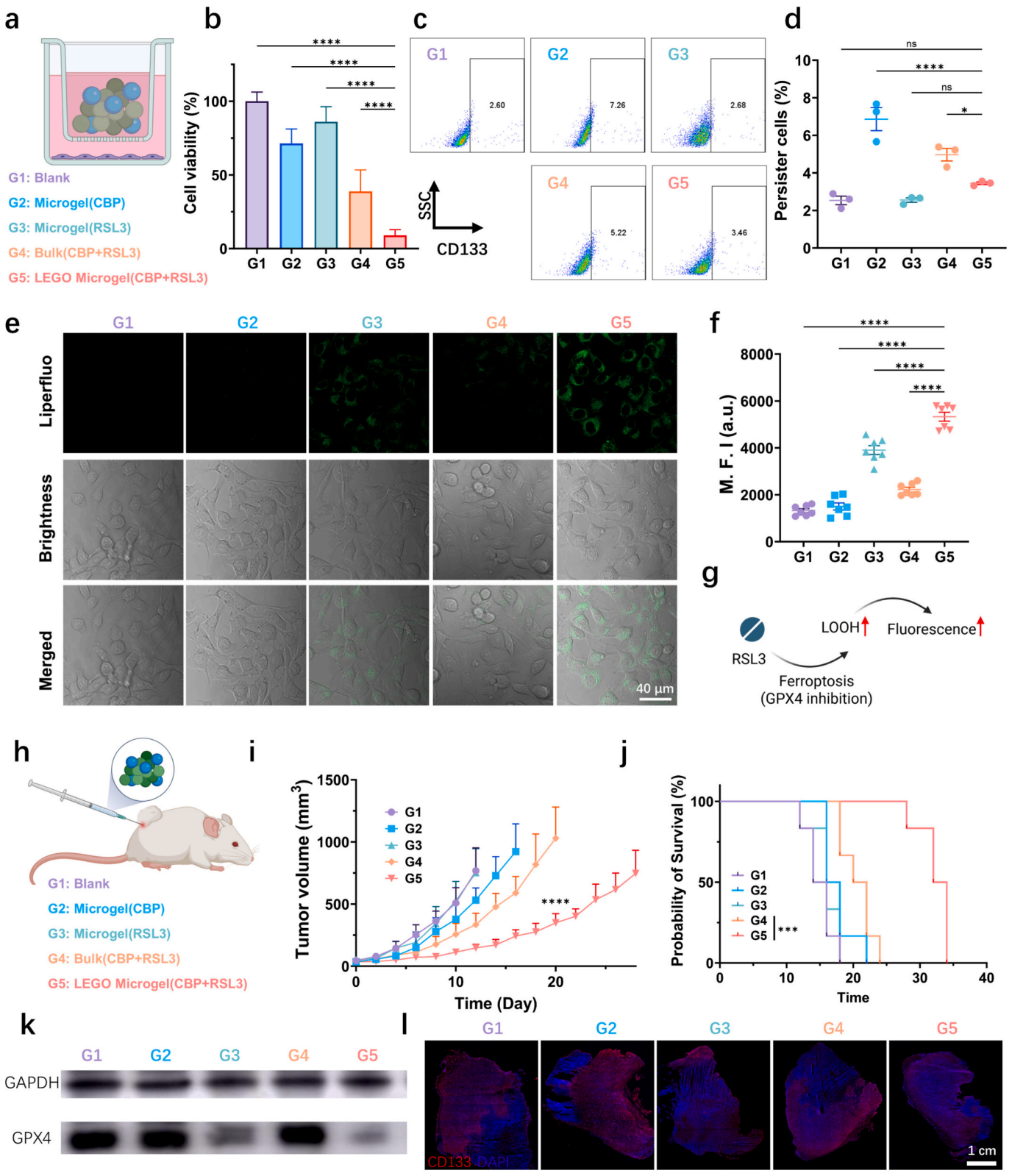

Fig. 4. LEGO microgel to overcome drug resistance. (a) A schematic illustration showing the experiment in Transwell chambers. (b) Relative viabilities of 4 T1 cells after incubation with different microgels for 48 h (n = 3). (c, d) Representative flow cytometry plots (c) and statistical percentages (d) of persister cells ($CD133^{+}$) in 4 T1 cells after treated with different microgels (n = 3). (e, f) The confocal images (e) and quantitative analysis of LiperFluo fluorescence intensity (f) of 4 T1 cells treated with different microgels ($n = 7$). (g) Illustration showing the process of RSL3 to produce lipid peroxides detected by LiperFluo. (h) The schematic illustration showing the design of treatment in vivo. (i, j) Tumor growth curve (i) and survival rate (j) of mice with different treatments ($n = 6$). (k) Western blot analysis of GPX4 expression in tumors under different treatments. (l) The immunofluorescence imaging of anti-$CD133^{+}$ stained tumor slices collected from mice in different groups. The data are presented as mean ± sem, and P values were calculated by one-way ANOVA with Tukey's post hoc test, while in Figure j, statistical analysis was performed using log-rank (Mantel–Cox) test, $^{*}p < 0.05$, $^{***}p < 0.001$,$^{****}p < 0.0001$.

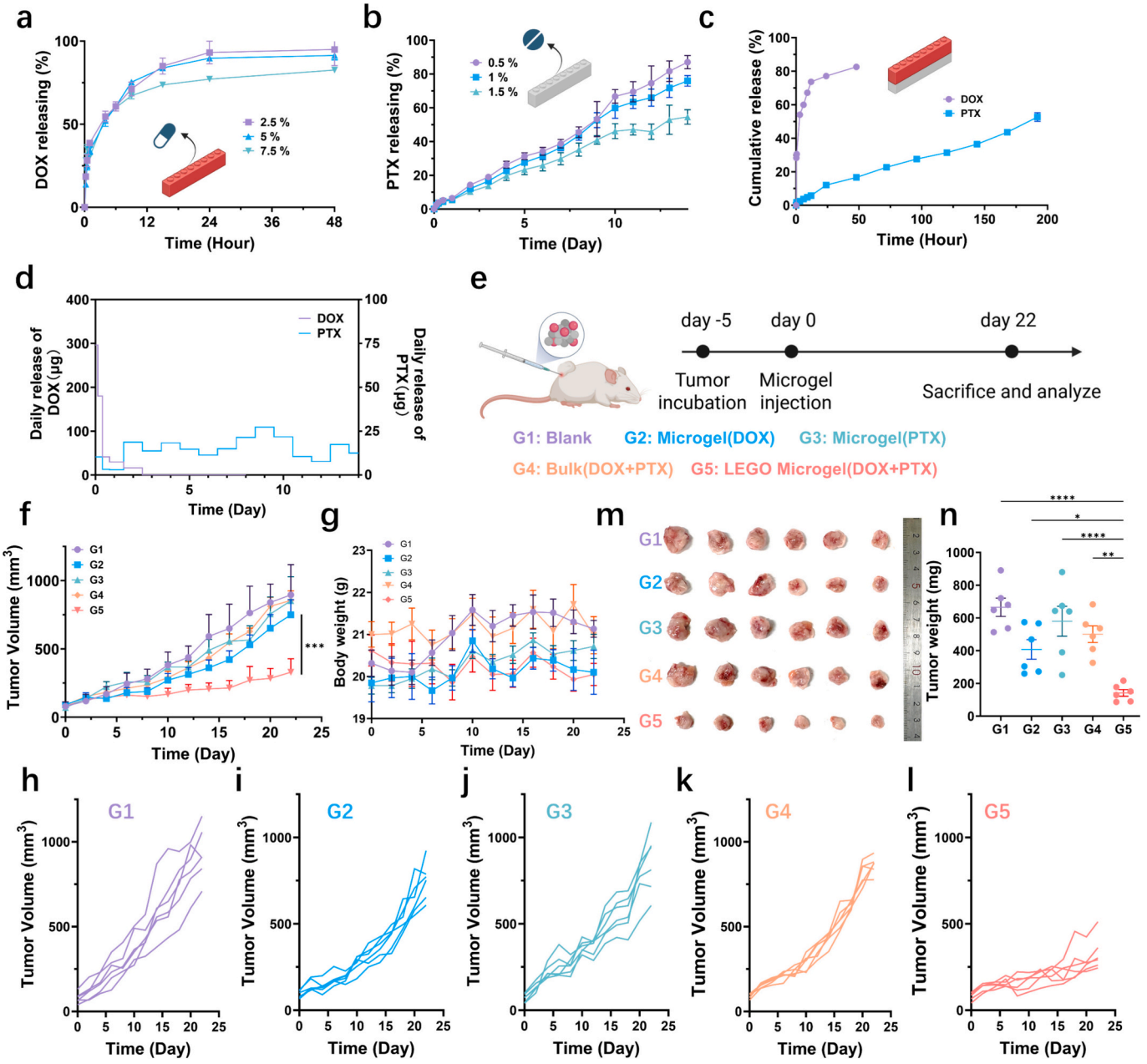

Fig. 5. The antitumor efficacy of LEGO microgel. (a) The release curves of doxorubicin from GelMA microgel with different concentrations (n = 3). (b) The release curves of paclitaxel from ALG microgel with different concentrations (n = 3). (c) The release of doxorubicin and paclitaxel from LEGO microgel (n = 3). (d) Daily drug release from LEGO microgel. (e) The schematic illustration showing the design and timeline of in vivo experiment. (f, g) Tumor growth curve (f) and body weight (g) of mice with different treatments (n = 6). (h, i) The photograph (h) and weight (i) of tumors collected on day 22 after different treatments (n = 6). (j-n) Individual tumor growth curves in different groups. The data are presented as mean ± sem, and *P* values were calculated by one-way ANOVA with Tukey's post hoc test, $^{*}p < 0.05$, $^{**}p < 0.01$, $^{***}p < 0.001$, $^{****}p < 0.0001$.

system's excellent biocompatibility and minimal systemic toxicity. Terminal analysis of excised tumors provided compelling morphological evidence, with the LEGO Microgel(DOX + PTX) group exhibiting both the smallest tumor volume and lightest tumor weight (Fig. 5m, n), providing robust in vivo validation of our platform's ability to synergize drug sequence and release kinetics for enhanced antitumor efficacy.

2. Conclusion

In summary, we have pioneered an innovative LEGO-inspired modular microgel platform that addresses a central challenge in drug delivery: the lack of independent and programmable control over multiple drug release kinetics within a single formulation. Our approach revolutionizes conventional hydrogel systems by decoupling drug loading and release into distinct, independently optimized microsphere modules, thereby overcoming a critical limitation of conventional monolithic hydrogels: the inability to precisely coordinate release kinetics for multiple drugs with disparate properties. The breakthrough of our system stems from its modular architecture and programmable assembly. We have demonstrated that the release profile of each drug—regardless of hydrophilicity—can be precisely engineered by modulating the matrix concentration of its dedicated module. Subsequent physical integration of these pre-programmed modules into an injectable microgel seamlessly translates independent release curves into sophisticated, temporally controlled delivery from a single administration. We rigorously validated this platform in two clinically relevant

scenarios. First, it enabled sequential delivery of carboplatin and RSL3 to effectively overcome chemotherapy resistance through a novel "induce-and-eradicate" strategy against persister cells, an achievement unattainable with conventional bulk hydrogel. Second, its reconfiguration successfully replicated the clinical DOX → PTX sequential regimen with enhanced antitumor efficacy. These results demonstrate that the modular microgel functions not merely as a carrier, but as a temporal regulator of drug action, enabling therapeutic outcomes unattainable with conventional formulations. Looking forward, this modular platform demonstrates significant potential for scalable manufacture and clinical translation. The fundamental building blocks—such as microfluidic-generated GelMA microspheres and electrosprayed ALG microspheres—are fabricated using inherently scalable techniques. A particularly advantageous feature of this modular architecture is the ability to independently produce and store drug-loaded modules in bulk, which can then be rapidly assembled into customized therapeutic formulations via simple physical mixing. This design enables precise customization of combination therapies and coordinated control over drug release kinetics (e.g., sequential delivery of chemo-immunotherapy regimens). Such operational flexibility makes this platform particularly well-suited for clinical implementation of complex, multi-agent therapeutic strategies.

CRediT authorship contribution statement

Zhisheng Xiao: Writing – review & editing, Writing – original draft, Visualization, Validation, Software, Resources, Project administration, Methodology, Investigation, Formal analysis, Data curation, Conceptualization. **Zhiqiang Wu:** Visualization, Resources, Project administration, Methodology, Data curation. **Qiaofeng Li:** Validation, Resources, Project administration, Methodology, Data curation. **Yu Miao:** Resources, Project administration, Methodology, Investigation, Data curation. **Nan Wang:** Resources, Project administration, Methodology. **Yifang Yang:** Resources, Project administration, Conceptualization. **Qian Chen:** Writing – review & editing, Supervision, Resources, Investigation, Funding acquisition. **Yang Yang:** Writing – review & editing, Supervision, Resources, Investigation, Funding acquisition.

Declaration of competing interest

The authors declare no conflict of interest.

Acknowledgments

This article was partially supported by the National Research Programs of China (2022YFA1206500), the National Natural Science Foundation of China (52450010, 52325106, 52271248), the Collaborative Innovation Center of Suzhou Nano Science and Technology, the Suzhou Key Laboratory of Nanotechnology and Biomedicine and the 111 Program from the Ministry of Education of China.

Appendix A. Supplementary data

Supplementary data to this article can be found online at https://doi.org/10.1016/j.jconrel.2026.114830.

Data availability

Data will be made available on request.

References

[1] S. Dong, S. An, Q. Saiding, Q. Chen, B. Liu, N. Kong, W. Chen, W. Tao, Therapeutic Hydrogels: Properties and Biomedical Applications, Chem. Rev. 125 (2025) 8835–8920, https://doi.org/10.1021/acs.chemrev.5c00182.
[2] H. Guo, T. Nakajima, D. Hourdet, A. Marcellan, C. Creton, W. Hong, T. Kurokawa, J.P. Gong, Hydrophobic Hydrogels with Fruit-Like Structure and Functions, Adv. Mater. 31 (2019) 1900702, https://doi.org/10.1002/adma.201900702.
[3] J. Li, D.J. Mooney, Designing hydrogels for controlled drug delivery, Nat. Rev. Materi. 1 (2016) 16071, https://doi.org/10.1038/natrevmats.2016.71.
[4] A.C. Daly, L. Riley, T. Segura, J.A. Burdick, Hydrogel microparticles for biomedical applications, Nat. Rev. Materi. 5 (2020) 20–43, https://doi.org/10.1038/s41578-019-0148-6.
[5] K. Zhang, Q. Feng, Z. Fang, L. Gu, L. Bian, Structurally Dynamic Hydrogels for Biomedical Applications: Pursuing a Fine Balance between Macroscopic Stability and Microscopic Dynamics, Chem. Rev. 121 (2021) 11149–11193, https://doi.org/10.1021/acs.chemrev.1c00071.
[6] J. Zhang, C. Li, H. Liu, Q. Wang, A.Y. Xu, K. Shah, L. Qi, Z. Wang, X. Zhang, C. Huang, C. Lei, S. Liu, L. Yue, H. Sun, Hydrogel delivery systems in intervertebral disc degeneration: Current status and future perspectives, J. Control. Release 386 (2025) 114066, https://doi.org/10.1016/j.jconrel.2025.114066.
[7] W. Shi, X. Ying, X. Sheng, S. Das, D. He, K. Collins, Y. Hu, M.G. Finn, Injectable Hydrogels for Programmable Nanoparticle Release, Adv. Funct. Mater. 35 (2025) 2409796, https://doi.org/10.1002/adfm.202409796.
[8] C. Lou, X. Tian, H. Deng, Y. Wang, X. Jiang, Dialdehyde-β-cyclodextrin-crosslinked carboxymethyl chitosan hydrogel for drug release, Carbohydr. Polym. 231 (2020) 115678, https://doi.org/10.1016/j.carbpol.2019.115678.
[9] Y. Han, J. Yang, W. Zhao, H. Wang, Y. Sun, Y. Chen, J. Luo, L. Deng, X. Xu, W. Cui, H. Zhang, Biomimetic injectable hydrogel microspheres with enhanced lubrication and controllable drug release for the treatment of osteoarthritis, Bioact. Mater. 6 (2021) 3596–3607, https://doi.org/10.1016/j.bioactmat.2021.03.022.
[10] R.M. Webster, Combination therapies in oncology, Nat. Rev. Drug Discov. 15 (2016) 81–82, https://doi.org/10.1038/nrd.2016.3.
[11] P. Sidaway, New combination therapy for advanced-stage RCC, Nat. Rev. Clin. Oncol. 20 (2023) 353, https://doi.org/10.1038/s41571-023-00765-y.
[12] M. Gosecka, M. Gosecki, D. Jaworska-Krych, Hydrophobized Hydrogels: Construction Strategies, Properties, and Biomedical Applications, Adv. Funct. Mater. 33 (2023) 2212302, https://doi.org/10.1002/adfm.202212302.
[13] Z. Li, G. Li, J. Xu, C. Li, S. Han, C. Zhang, P. Wu, Y. Lin, C. Wang, J. Zhang, X. Li, Hydrogel Transformed from Nanoparticles for Prevention of Tissue Injury and Treatment of Inflammatory Diseases, Adv. Mater. 34 (2022) 2109178, https://doi.org/10.1002/adma.202109178.
[14] L. Wu, J. Li, Y. Wang, X. Zhao, Y. He, H. Mao, W. Tang, R. Liu, K. Luo, Z. Gu, Engineered Hierarchical Microdevices Enable Pre-Programmed Controlled Release for Postsurgical and Unresectable Cancer Treatment, Adv. Mater. 35 (2023) 2305529, https://doi.org/10.1002/adma.202305529.
[15] X. Chen, T. Chen, L. Ren, G. Chen, X. Gao, G. Li, X. Zhu, Triplex DNA Nanoswitch for pH-Sensitive Release of Multiple Cancer Drugs, ACS Nano 13 (2019) 7333–7344, https://doi.org/10.1021/acsnano.9b03846.
[16] S. Correa, A.K. Grosskopf, J.H. Klich, H. Lopez Hernandez, E.A. Appel, Injectable liposome-based supramolecular hydrogels for the programmable release of multiple protein drugs, Matter 5 (2022) 1816–1838, https://doi.org/10.1016/j.matt.2022.03.001.
[17] J. Chen, X. Gan, S. Su, S. Jiao, Z. Gong, Z. Liu, X. Wu, J. Jiang, J. Zhang, J. Wan, Conditional sequential delivery of ginkgetin and rapamycin orchestrates inflammation and autophagy to alleviate intervertebral disc degeneration, J. Control. Release 381 (2025) 113556, https://doi.org/10.1016/j.jconrel.2025.02.052.
[18] J. Han, Z. Wu, S. Zhan, T. Sheng, J. You, J. Yu, J. Fu, Y. Zhang, Z. Gu, Biorhythm-mimicking growth hormone patch, Nat. Mater. 24 (2025) 1283–1294, https://doi.org/10.1038/s41563-025-02188-9.
[19] P. Xu, T.-T. Li, B.-C. Wang, Y.-J. Yi, W.-C. Zhang, G.-D. Sun, Y. Zhang, Z.-Z. Li, Supramolecular assemblies with spatio-temporal sequential drug delivery capability treat spinal cord injury *via* neuroprotection and immunoregulation, J. Control. Release 360 (2023) 528–548, https://doi.org/10.1016/j.jconrel.2023.07.008.
[20] T.F. Stewart, N.V. Kotha, H.E. Dzimitrowicz, D. Makrakis, A.R. Khaki, N.I. Simon, A.A. Nelson, D. Freeman, T.L. Rose, W. Beck, N.S. Chawla, S.K. Pal, D. Kilari, M. I. Milowsky, A.B. Apolo, P. Grivas, T. Zhang, G.P. Sonpavde, R.R. McKay, Efficacy of anti-PD(L)1 therapy for patients (Pts) with advanced urothelial carcinoma (aUC) with primary resistance to platinum-based chemotherapy (PC), J. Clin. Oncol. 39 (2021) e16515, https://doi.org/10.1200/JCO.2021.39.15_suppl.e16515.
[21] L. Gianni, L. Viganò, A. Locatelli, G. Capri, A. Giani, E. Tarenzi, G. Bonadonna, Human pharmacokinetic characterization and in vitro study of the interaction between doxorubicin and paclitaxel in patients with breast cancer, J. Clin. Oncol. 15 (1997) 1906–1915, https://doi.org/10.1200/JCO.1997.15.5.1906.
[22] M.D.T. de Melo, A.L.C. Almeida, A.J.O.M. de Neto, E.G.S. dos Júnior, I.C. Reis, L. Mota, N.L. Lopes, S.O. De Afonseca, T.M. do Espírito Santo, Which therapeutic strategy is less cardiotoxic in the treatment of breast cancer: Using paclitaxel before or after doxorubicin? J. Clin. Oncol. 39 (2021) e12617, https://doi.org/10.1200/JCO.2021.39.15_suppl.e12617.
[23] M. Kciuk, A. Gielecińska, S. Mujwar, D. Kołat, Ż. Kałuzińska-Kołat, I. Celik, R. Kontek, Doxorubicin—An Agent with Multiple Mechanisms of Anticancer Activity, Cells 12 (2023) 659, https://doi.org/10.3390/cells12040659.
[24] T.H. Wang, H.S. Wang, Y.K. Soong, Paclitaxel-induced cell death: where the cell cycle and apoptosis come together, Cancer 88 (2000) 2619–2628, https://doi.org/10.1002/1097-0142(20000601)88:11%253C2619::aid-cncr26%253E3.0.co;2-j.
[25] GPX4 Inhibition Selectively Targets Drug-Tolerant Persister Cells, Cancer Discov. 8 (2018) OF9, https://doi.org/10.1158/2159-8290.CD-RW2017-215.

[26] V. Brabec, J. Kasparkova, Molecular aspects of resistance to antitumor platinum drugs, Drug Resist. Updat. 5 (2002) 147–161, https://doi.org/10.1016/S1368-7646(02)00047-X.
[27] H. Kalkavan, M.J. Chen, J.C. Crawford, G. Quarato, P. Fitzgerald, S.W.G. Tait, C. R. Goding, D.R. Green, Sublethal cytochrome c release generates drug-tolerant persister cells, Cell 185 (2022) 3356–3374.e22, https://doi.org/10.1016/j.cell.2022.07.025.
[28] C. Pottier, L. Montero-Ruiz, R. Jehay, C. Wery, D. Baiwir, G. Mazzucchelli, S. Bekisz, R. Thissen, C. Josse, A. Rorive, S. Gofflot, A. Dahmani, L. Morisset, J. Collignon, P. Delvenne, E. Marangoni, A. Noël, G. Jerusalem, N.E. Sounni, Targeting ferroptosis resistance resensitizes metastatic HR+HER2− breast cancer cells to palbociclib-hormone therapy, Cancer Communicat. 45 (2025) 460–464, https://doi.org/10.1002/cac2.12646.
[29] G. Liu, X. Yuan, Z. Zeng, P. Tunici, H. Ng, I.R. Abdulkadir, L. Lu, D. Irvin, K. L. Black, J.S. Yu, Analysis of gene expression and chemoresistance of CD133+ cancer stem cells in glioblastoma, Mol. Cancer 5 (2006) 67, https://doi.org/10.1186/1476-4598-5-67.
[30] I.S. Bryukhovetskiy, Y. Khotimchenko, V. Shevchenko, 11P - Molecular determinants of interaction between glioblastoma CD133+ cancer stem cells and extracellular matrix, Ann. Oncol. 30 (2019) vii4, https://doi.org/10.1093/annonc/mdz413.016.
[31] D. Burgos-Ojeda, B.R. Rueda, R.J. Buckanovich, Ovarian cancer stem cell markers: Prognostic and therapeutic implications, Cancer Lett. 322 (2012) 1–7, https://doi.org/10.1016/j.canlet.2012.02.002.
[32] K. Yamanaka, Y. Saito, J. Sakiyama, Y. Ohuchi, F. Oseto, N. Noguchi, A novel fluorescent probe with high sensitivity and selective detection of lipid hydroperoxides in cells, RSC Adv. 2 (2012) 7894–7900, https://doi.org/10.1039/C2RA20816D.
[33] S. Loibl, P. Poortmans, M. Morrow, C. Denkert, G. Curigliano, Breast cancer, Lancet 397 (2021) 1750–1769, https://doi.org/10.1016/S0140-6736(20)32381-3.
[34] E. Alanya Rodríguez, C. Falo Zamora, M.J. Gil Gil, P. Anna, R. Ortega, A. Fernandez, I. Morilla, A. Stradella, S. Cobo, S. Pernas Simon, Efficacy of taxanes followed by anthracyclines as neoadjuvant therapy in HER2-negative breast cancer (BC): Analysis of everyday clinical practice, J. Clin. Oncol. 35 (2017) e12112, https://doi.org/10.1200/JCO.2017.35.15_suppl.e12112.
[35] R. Gray, R. Bradley, J. Braybrooke, Z. Liu, R. Peto, L. Davies, D. Dodwell, P. McGale, H. Pan, C. Taylor, W. Barlow, J. Bliss, P. Bruzzi, D. Cameron, G. Fountzilas, S. Loibl, J. Mackey, M. Martin, L. Del Mastro, V. Möbus, V. Nekljudova, S. De Placido, S. Swain, M. Untch, K.I. Pritchard, J. Bergh, L. Norton, C. Boddington, J. Burrett, M. Clarke, C. Davies, F. Duane, V. Evans, L. Gettins, J. Godwin, R. Hills, S. James, H. Liu, E. MacKinnon, G. Mannu, T. McHugh, P. Morris, S. Read, Y. Wang, Z. Wang, P. Fasching, N. Harbeck, P. Piedbois, M. Gnant, G. Steger, A. Di Leo, S. Dolci, P. Francis, D. Larsimont, J. M. Nogaret, C. Philippson, M. Piccart, S. Linn, P. Peer, V. Tjan-Heijnen, S. Vliek, J. Mackey, D. Slamon, J. Bartlett, V.H. Bramwell, B. Chen, S. Chia, K. Gelmon, P. Goss, M. Levine, W. Parulekar, J. Pater, E. Rakovitch, L. Shepherd, D. Tu, T. Whelan, D. Berry, G. Broadwater, C. Cirrincione, H. Muss, R. Weiss, Y. Shan, Y. F. Shao, X. Wang, B. Xu, D.-B. Zhao, H. Bartelink, N. Bijker, J. Bogaerts, F. Cardoso, T. Cufer, J.-P. Julien, P. Poortmans, E. Rutgers, C. van de Velde, E. Carrasco, M. A. Segui, J.U. Blohmer, S. Costa, B. Gerber, C. Jackisch, G. von Minckwitz, M. Giuliano, M. De Laurentiis, C. Bamia, G.-A. Koliou, D. Mavroudis, R. A'Hern, P. Ellis, L. Kilburn, J. Morden, J. Yarnold, M. Sadoon, A.H. Tulusan, S. Anderson, G. Bass, J. Costantino, J. Dignam, B. Fisher, C. Geyer, E.P. Mamounas, S. Paik, C. Redmond, D.L. Wickerham, M. Venturini, C. Bighin, S. Pastorino, P. Pronzato, M.R. Sertoli, T. Foukakis, K. Albain, R. Arriagada, E. Bergsten Nordström, F. Boccardo, E. Brain, L. Carey, A. Coates, R. Coleman, C. Correa, J. Cuzick, N. Davidson, M. Dowsett, M. Ewertz, J. Forbes, R. Gelber, A. Goldhirsch, P. Goodwin, D. Hayes, C. Hill, J. Ingle, R. Jagsi, W. Janni, H. Mukai, Y. Ohashi, L. Pierce, V. Raina, P. Ravdin, D. Rea, M. Regan, J. Robertson, J. Sparano, A. Tutt, G. Viale, N. Wilcken, N. Wolmark, W. Wood, M. Zambetti, Increasing the dose intensity of chemotherapy by more frequent administration or sequential scheduling: a patient-level meta-analysis of 37 298 women with early breast cancer in 26 randomised trials, Lancet 393 (2019) 1440–1452, https://doi.org/10.1016/S0140-6736(18)33137-4.